

PCCP

Accepted Manuscript



This is an *Accepted Manuscript*, which has been through the Royal Society of Chemistry peer review process and has been accepted for publication.

Accepted Manuscripts are published online shortly after acceptance, before technical editing, formatting and proof reading. Using this free service, authors can make their results available to the community, in citable form, before we publish the edited article. We will replace this *Accepted Manuscript* with the edited and formatted *Advance Article* as soon as it is available.

You can find more information about *Accepted Manuscripts* in the [Information for Authors](#).

Please note that technical editing may introduce minor changes to the text and/or graphics, which may alter content. The journal's standard [Terms & Conditions](#) and the [Ethical guidelines](#) still apply. In no event shall the Royal Society of Chemistry be held responsible for any errors or omissions in this *Accepted Manuscript* or any consequences arising from the use of any information it contains.

Variable-composition Structural Optimization and Experimental Verification of MnB₃ and MnB₄

Haiyang Niu,^{a, b} Xing-Qiu Chen,^{*a} Weijun Ren,^a Qiang Zhu,^c Artem R. Oganov,^{c, b, d} Dianzhong Li^a and Yiyi Li^a

Received Xth XXXXXXXXXXXX 20XX, Accepted Xth XXXXXXXXXXXX 20XX

First published on the web Xth XXXXXXXXXXXX 200X

DOI: 10.1039/b000000x

In combination with the variable-composition evolutionary algorithm calculations and the first-principles calculations, we have systematically searched for all the stable compounds and their crystal structures in the extensively investigated binary Mn-B system. Our results have uncovered four viable ground state compounds, with Mn₂B, MnB, MnB₄ and previously never reported MnB₃ and two metastable compounds, MnB₂ and Mn₃B₄. Our calculations demonstrated that the early characterized *mC10* structure of MnB₄ showed dynamical instability with large imaginary phonon frequencies and instead, a new *mP20* structure is predicted to be stable both dynamically and thermodynamically, with a considerable energy gain and no imaginary phonon frequencies. The new MnB₃ compound crystallizes in the monoclinic *mC16* structure which lies 3.2 meV/atom below the MnB (*oP8*) ↔ MnB₄ (*mP20*) tie-line at *T* = 0 K. Furthermore, these proposed phases have been verified by our annealed samples after the arc-melting synthesis and the corresponding powder XRD measurements.

1 Introduction

The fast development of the structural prediction methods^{1,2} within the first-principles framework of density functional theory (DFT) has resulted in extremely successful progresses, such as materials discoveries of novel boron phase (γ -B₂₈)³, Li-ion batteries⁴, thermoelectric material⁵, topological insulators⁶, superhard carbon allotropes⁷, and so on. Recently, those methods have been extensively applied to transition metal borides (*i.e.* WB_{3+x}⁸⁻¹¹, CrB₄¹², ReB₂¹³⁻¹⁶, OsB₂^{17,18}, FeB₄^{16,19,20}, and CaB₆²¹) due to their promising properties, such as facile synthesis at ambient pressure, superior mechanical properties, and good electrical conductivity. Among them, manganese borides are well known for their interesting mechanical properties and have been extensively studied, both experimentally and theoretically²²⁻³⁴.

In the early study²⁷, the compound of MnB₄ was experimentally demonstrated to crystallize in the *mC10* structure. This structure is characteristic of the three-dimensional (3D) framework of boron with the interconnected square B₄ unit,

which is highly similar to that in the early experimentally proposed *oI10* structure of CrB₄. Recently, this *mC10* phase was even predicted to exhibit the outstanding mechanical properties with an estimated Vickers hardness as high as 49.9 GPa³² and high ideal strengths, highlighting its potential application³³. Interestingly, most recently, the square B₄ unit in the *oI10* structure of CrB₄ was demonstrated, both theoretically and experimentally, to be not correct and it spontaneously undergoes a distortion into the low-symmetry *oP10* phase¹². Therefore, we also suspected whether or not the previously recognized *mC10*-MnB₄ structure is correct. In addition, a *hP6* (ReB₂-type) phase has been recently proposed as a ground state phase of MnB₂²⁹ and it was further suggested to be superhard³⁰. Even though plenty of studies to synthesize this *hP6* phase, none of them succeeded to achieve it^{29,31}. We also noted that in a recent experimental investigation³¹ an unidentified phase called MnB_x has been proposed, experimentally. Within this context, it is highly desirable to carefully revisit the Mn-B binary system by employing a recently developed variable-composition evolutionary calculations within the density functional theory and some proper experimental characterizations.

2 Methods

In order to identify ambient-condition stable ground state compositions and structures of the binary manganese-boron system, we have employed the variable-composition evolutionary algorithm, recently implemented in the USPEX

^a Shenyang National Laboratory for Materials Science, Institute of Metal Research, Chinese Academy of Sciences, Shenyang 110016, China Fax: +86-24-23971429; Tel: +86-24-83970102; E-mail: xingqiu.chen@imr.ac.cn

^b Moscow Institute of Physics and Technology, 9 Institutskiy Lane, Dolgoprudny city, Moscow Region 141700, Russia

^c Department of Geosciences, Center for Materials by Design, and Institute for Advanced Computational Science, State University of New York, Stony Brook, NY 11794-2100.

^d School of Materials Science, Northwestern Polytechnical University, Xian 710072, China

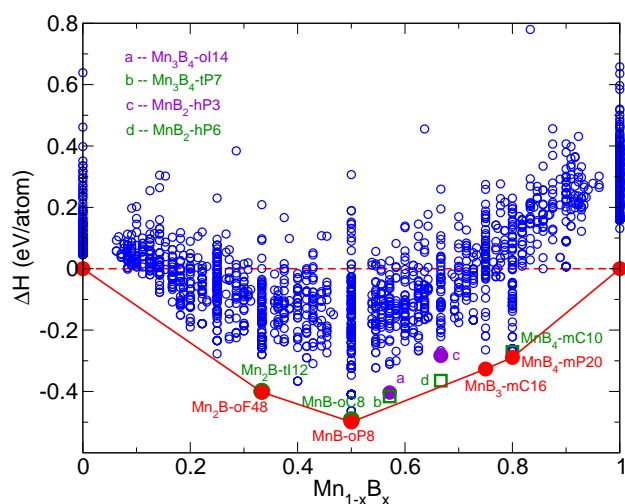


Fig. 1 The derived enthalpies of formation predicted by variable-composition evolutionary computations for the Mn-B system. Every circles represents an individual structure and the most stable ground state phases (red circles) are connected to form the convex hull.

code^{1,35–38} in coupling with the first-principles calculations within the framework of density functional theory (the Vienna *Ab initio* Simulation Package VASP)^{39,40} for the determinations of the total energies, optimized lattice structures and their corresponding electronic structures. For first-principles calculations we employed all electron projector augmented wave method and the generated gradient approximation⁴¹ for the exchange-correlation energy including the approach of Vosko, Wilk and Nusair for spin polarized systems⁴², along with a plane-wave cutoff energy of 500 eV and dense Monkhorst-Pack k-point meshes⁴³ (with a reciprocal space resolution of $2\pi \times 0.03\text{\AA}^{-1}$). The formation enthalpy of the compound of Mn_xB_y is derived with respect to the ground state phases of $\alpha\text{-B}$ ⁴⁴ and $\alpha\text{-Mn}$ ⁴⁵. In addition, for the structural candidates searched by USPEX we further derived phonon dispersions using the finite-displacement approach as implemented in the FROPHO code⁴⁶ to clarify the structural stabilities.

Besides theoretical predictions, we have further performed some necessary experiments. A 20g sample with the initial atomic ratio of $\text{B}/\text{Mn} = 3$ was prepared by repeated arc-melting of electrolytic manganese (from Alfa Aesar, claimed purity 99.997%) and crystalline boron pieces (from Alfa Aesar, claimed purity 99.5%) under argon atmosphere. Based on the analysis of the phase diagram of the Mn-B system^{22,28}, we have divided the samples into two groups for different treatments. For No.1 sample, no heat treatment was adopted after melting. For No.2 sample, it was sealed in quartz under argon atmosphere first and then annealed in a high temperature furnace for 336 hours at 1000 °C. The samples were char-

acterized via scanning electron microscope (SEM, HITACHI S-3400N) in the back-scattered electron mode (BSE). Finally, the XRD patterns for the two samples were obtained using a Rigaku diffractometer with $\text{Cu } K_\alpha$ irradiation ($\lambda = 1.54056 \text{\AA}$).

3 Results and Discussions

3.1 First-principles calculations

According to the latest Mn-B phase diagram²², there exist five compounds Mn_2B (Mg_2Cu type, *oF48*, $Fddd$ ^{23,24}; Al_2Cu type, *tI12*, $I4/mcm$ ²⁵), MnB (CrB type, *oC8*, $Cmcm$; FeB type, *oP8*, $Pnma$ ²⁵), Mn_3B_4 (Ta_3B_4 type, *tP7*, $Immm$ ²⁵), MnB_2 (AlB_2 type, *hP3*, $P6/mmm$ ²⁶), and MnB_4 (*mC10*, $C2/m$ ²⁷). Among them, MnB_2 is a high-temperature phase which can only be synthesized above 1100 °C²², which was recently confirmed again³⁴. Figure 1 compiles the DFT formation enthalpies of compounds searched by the variable-composition evolutionary algorithm in USPEX at $T = 0 \text{ K}$ for the $\text{Mn}_{1-x}\text{B}_x$ ordered structures. For the most stable ground state phase, we drawn the convex hull in Fig. 1 connecting $\alpha\text{-Mn}$, Mn_2B (*oF48*), MnB (*oI14*), MnB_3 (*mC16*) and MnB_4 (*mP20*), and $\alpha\text{-B}$. Several aspects can be summarized as follows,

1) Mn_2B and MnB : In nice agreement with the experimental findings^{22–25,47,48}, our calculations reproduced successfully the experimentally observed structures and compositions for both Mn_2B and MnB (*c.f.*, Table 1). Mn_2B is found to crystallize in the *oF48* ground state phase with a derived enthalpy of -0.41 eV/atom lower than the *tI12* phase and MnB has an *oP8* energy-lowest phase, but with an enthalpy of -0.50 eV/atom which is just slight lower by 7 meV than that of the *oC8* phase. The spin-polarized calculations further revealed that the *oF48* phase of Mn_2B is nonmagnetic. However, both *oC8* and *oP8* phases of MnB is found to be ferromagnetic with the local spin moments of Mn being $1.9 \mu_B/\text{atom}$ and $2.0 \mu_B/\text{atom}$, respectively. And our result is in good agreement with previously experimental investigation of the magnetic moment, $1.83 \mu_B$ of Mn in *oP8* MnB ⁴⁹.

2) Mn_3B_4 and MnB_2 : According to our GGA-level calculations the previously experimentally synthesized Mn_3B_4 and MnB_2 are found to be metastable since their lowest-enthalpy phases are above the convex hull as shown in Fig. 1. For Mn_3B_4 , the experimentally reported *oI14* phase is 0.014 eV/atom less stable in energy than the *tP7* phase. Interestingly, this *tP7* phase crystallizes in the tetragonal structure with a space group of $P4m2$ (*c.f.*, Table 1). In particular, it needs to be emphasized that the *oI14* phase was reported to be antiferromagnetic, in the disagreement with our spin-polarized calculations. Our results demonstrated that the antiferromagnetic *oI14* phase is unstable dynamically because its phonon

dispersion exhibits largely imaginary. In contrast, our results reveal that both *oI14* and *oP7* phases are in the ferromagnetic ordering with the nearly same magnetic moment of $1.9 \mu_B$ per Mn.

For MnB_2 , our GGA-level computations found that the most stable phase is the *hP16* (ReB_2 -type) phase with an enthalpy of about -0.36 eV/atom much lower than the *hP3* (AlB_2 -type) phase. This result is in nice agreement with the previous first-principles calculations^{30,32,34}. Our spin-polarized calculations also found that the *hP16* phase is non-magnetic whereas the *hP3* phase is antiferromagnetic, with the local spin moment of $2.4 \mu_B$ per Mn, being marginally consistent with the experimental data of $2.6 \mu_B$ ⁵³ obtained by neutron diffraction. Recently, Gou *et al* performed a GGA+U calculation on MnB_2 and found the *hP3* phase is stable over the *hP16* phase³⁴, interpreting the experimental formation of the *hP3* phase. But, the GGA+U calculations yielded a higher magnetic moment of $3.3 \mu_B$, much higher than the experimental data³⁴. Therefore, one would need to carefully estimate the artificial option of the correlation U effect of the Mn d -states within the DFT framework, which certainly affects its relative stability. However, to date the lowest-enthalpy nonmagnetic *hP16* phase at the GGA level has been never synthesized.

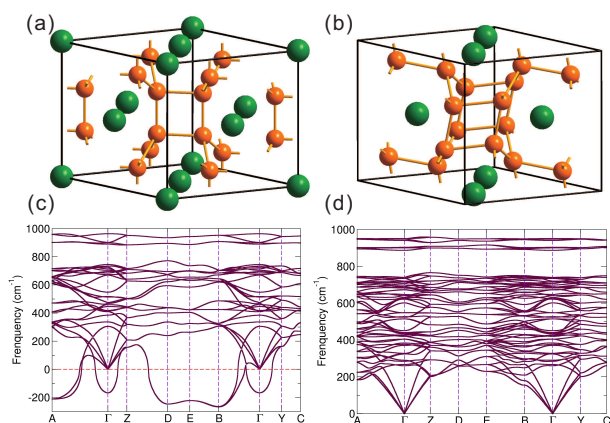


Fig. 2 The crystal structures and their phonon dispersions of MnB_4 : (a) the previously experimentally synthesized monoclinic *mC10* structure²⁷, (b) the USPEX searched theoretical monoclinic *mP20* structure, (c) the derived phonon dispersion of the *mC10* phase which is proven to be unstable, mechanically, and (d) the derived phonon dispersion of the *mP20* phase that is stable, both mechanically and thermodynamically.

3) MnB_4 : From Fig. 1 the early experimentally proposed *mC10* phase²⁷ is uncovered to be thermodynamically less stable by 0.018 eV/atom than the currently theoretical found *mP20* phase with the space group of $P2_1/c$ (Table 1). As mentioned above, the *mC10* phase is built up by an unusual framework of interconnected square B_4 units (Fig. 2a), which is highly similar to the C_4 unit in the tetragonal body-centered

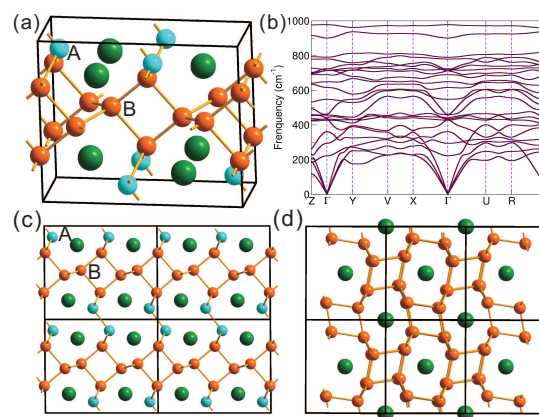


Fig. 3 (a) and (b) the *mC16* crystal structure of MnB_3 and its corresponding phonon dispersions, respectively. (c) and (d) the projections in the $2 \times 1 \times 2$ supercells along the b -axis of MnB_3 (*mC16*) and the $2 \times 2 \times 1$ supercells along the $(1\ 0\ -1)$ direction of MnB_4 (*mP20*), respectively. The boron atoms in the *mC16* phase can be classified into two types, one (marked by B with orange color) being fourfold coordinated with its nearest-neighboring (NN) boron atoms and the other one (marked by A with blue color) being threefold bounded with its NN boron atoms, whereas the boron atoms are all fourfold coordinated with its NN boron atoms in the *mP20* phase.

allotrope (bct-C_4 ⁵⁴) of carbon. Clearly, our derived phonon dispersion of this *mC10* phase demonstrates that it is indeed unstable, dynamically, because significant imaginary phonon frequencies have appeared, as evidenced in Fig. 2c. Interestingly, our calculations uncovered that the real crystal structure of MnB_4 is the *mP20* phase comprised of the distorted B_4 parallelogram units (Fig. 2b), showing a highly similar version to the most refined *oP10* phase of CrB_4 ¹². The phonon dispersions provide a robust evidence of the dynamical stability of the *mP20* phase, as illustrated in Fig. 2d.

We also noted that the same structure for MnB_4 , $P2_1/c$, has been proposed based on first principles calculations⁵⁰, and confirmed both by normal-pressure synthesized method⁵¹, and high-pressure, high-temperature synthesis technique⁵⁰. Interestingly, both FeB_4 and CrB_4 crystalline in the *oP10* structure, but the slight distortion of Mn site further reduces the symmetry of the unit cell of MnB_4 to the monoclinic *mP20* structure, which can be attributed to Peierls-Distortion⁵⁰⁻⁵².

The spin-polarized calculations further indicate that MnB_4 is nonmagnetic. The most recently published experimental work⁵⁰ showed that MnB_4 holds a paramagnetic effective moment of about $1.7 \mu_B$ above 150-200 K, and sizable effective moment and ferromagnetic spin correlations at 2 K by the magnetization measurements. This discrepancies can be mainly explained by the electron localization tendency on the Mn sites⁵⁰. Even though by introducing the effect of the on-

site Coulomb repulsions U , a small ferromagnetic moment about $0.6 \mu_B$ on Mn atoms can be obtained by the LSDA+ U method⁵⁰, the origin of the ferromagnetic spin correlations is highly puzzling.

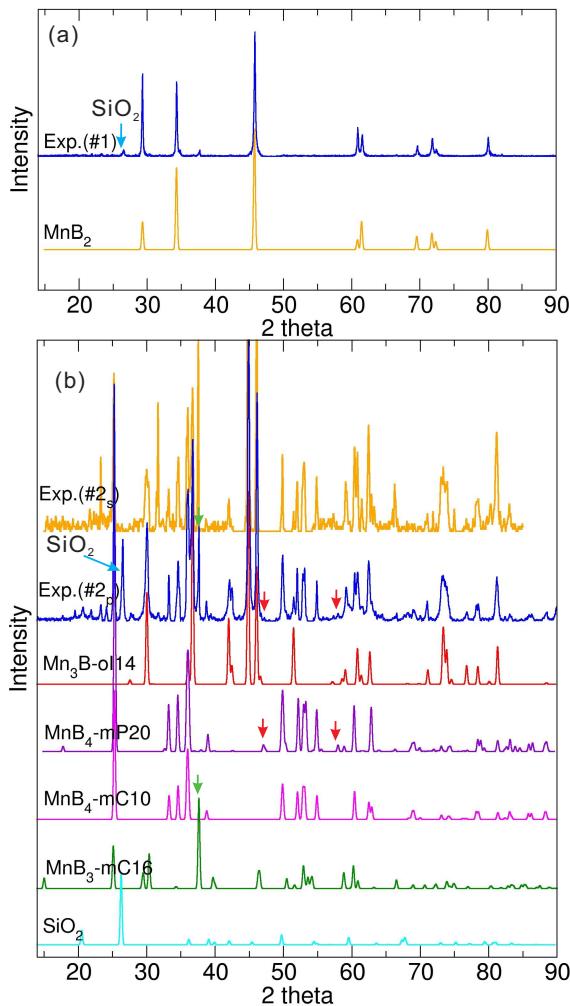


Fig. 4 Experimental and simulated x-ray diffraction patterns of (a) the as-cast No.1 sample: the experimental XRD pattern vs the theoretical one of MnB_2 , and (b) the annealed No.2 sample: the experimental pattern (2_s refers to surface XRD test and 2_p refers to powder XRD test) along with the theoretical ones of Mn_3B_4 ($hP3$), MnB_4 ($mP20$ and $mC10$), and MnB_3 ($mC16$). The peak at 26.4° corresponds to the impurity of SiO_2 .

4) MnB_3 : Our USPEX searches found a never observed MnB_3 phase to be thermodynamically stable with respect to the known compounds in Fig. 1 in the well-known Mn-B binary system. As illustrated in Fig. 3(a), MnB_3 crystallizes in the $mC16$ (C_2/m) structure (Table 1) and its phonon spectrum (Fig. 3b) show no any negative frequencies, thereby being stable, both dynamically and thermodynamically. In addition, the

spin-polarized calculations show that MnB_3 is nonmagnetic.

In particular, we would like to stress that the ground state $mC16$ phase of MnB_3 is indeed closely related with the $mP20$ phase of MnB_4 . As evidenced in Fig. 3(c and d), the projections along c -axis for both MnB_3 and MnB_4 clearly show that the boron framework in MnB_4 is composed of the 4+8 membered rings of boron atoms, whereas for MnB_3 the eight-membered boron rings have been broken due to the removal of one boron atom. This fact leaves some boron atoms (marked by A with blue color) in MnB_3 as coordinated by just three other boron atoms, compared with MnB_4 in which each boron atom is fourfold bonded with its nearest neighboring borons.

During the preparation process of this work, we have also recognized that, through the *ab initio* structure evolution (MAISE) code in combination with the largest *ab initio* database for metal borides, Geest and Kolmogorov also searched the Mn-B system⁵⁵. Besides the highly agreement with our current findings, they did not find the new phase of MnB_3 .

3.2 Experiments

The experimental powder XRD pattern of the No.1 as-cast arc-melting sample has been shown in Fig. 4(a). It can be seen that the XRD pattern of $hP3$ (AlB_2 -type) MnB_2 is in a good agreement with the experimental results, confirming the existence of the $hP3$ phase. Analyzing the microscopic structure as shown in Fig. 5, besides MnB_2 there is still some amorphous borons left in the sample, reflecting well the extra boron in our initial sample with a 3:1 B/Mn ratio. It is clear that the boron phase does not contribute obviously to the experimental XRD patterns. Although the $hP6$ phase of MnB_2 is revealed to be a ground state phase, our experiments did not observed its formation mainly because our samples have been synthesized under high temperature and then fastly quenched in the argon atmosphere. This fact has been already interpreted well by another recent first-principles calculation that suggested that the $hP6$ phase indeed becomes thermodynamically unstable above 747°C by deriving phonon free energies²⁹, in accordance with our current experimental synthesis at high temperature.

From the Mn-B binary phase diagram^{22,28}, MnB_2 would decompose into Mn_3B_4 and MnB_4 below 1100°C . In order to reproduce this process, the No. 2 sample was annealed at 1000°C for 336 hours. The SEM image shows a typical feature of eutectoid reaction with the lamellar patterns (Fig. 5). As revealed in the experimental powder XRD patterns, the existence of MnB_4 and Mn_3B_4 has been confirmed. In the first, our experiments confirmed the existence of the theoretically proposed $mP20$ phase and excluded the $mP20$ structure that was characterized by the previous XRD experiment²⁷. In particular, it needs to be mentioned that the simulated XRD pat-

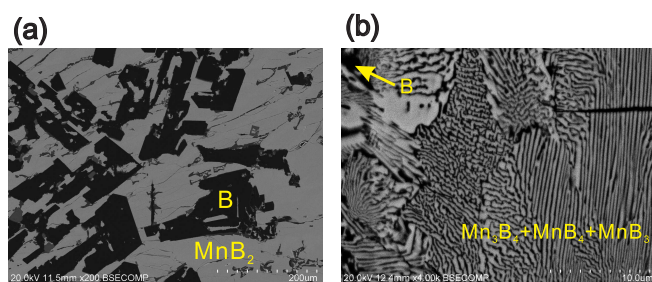


Fig. 5 (color online) EBSD micrograph images (a) the as-cast No.1 sample and (b) the annealed No.2 sample.

terns of both stable $mP20$ and unstable $mC10$ phases of MnB_4 are indeed very similar, except for two very tiny extra peaks at 2θ of 47.2° and 58.0° for the $mP20$ phase. As marked by two red arrows in Fig. 4b, the experimental XRD patterns exhibits these two small peaks, thereby providing the robust evidence of the appearance of $mP20$ phase in agreement with our current prediction. In the second, from the XRD patterns in Fig. 4b we still found the existing evidence of the never reported MnB_3 ($mC16$) phase. All its theoretical peaks match well with the experimental ones mostly matching together with those of MnB_4 and, in particular, the strongest peak at 37.8° shows a perfect agreement with the theoretically simulated peak of $mC16$ phase.

Here, we would like to emphasize that in a recent experimental investigation³¹ an unknown MnB_x was proposed based on the XRD peak at 26.4° , which is also precisely what is seen in our experimental patterns for both No.1 and No.2 samples (Fig. 4b). However, our analysis demonstrated that this peak at 26.4° originates from the impurity of SiO_2 introduced during the preparation of the powder of the samples polished using an agate mortar and pestle. To clarify this point, we have further performed a surface X-ray diffraction analysis for our No.2 annealed sample as shown in Fig. 4b, revealing the disappearance of the peak at 26.4° . Therefore, MnB_x defined in Ref.³¹ can be excluded safely.

4 Mechanical and electronic properties

Furthermore, Table 2 compiles the theoretically derived elastic constants (c_{ij}) of single crystals, the polycrystalline moduli (G , B , and E) according to the Voight-Reuss-Hill averages^{56–58}, Poisson's ratio (ν) and the estimated Vickers hardness (H_v) from our recently proposed empirical formula^{59–61} for these borides. It has been seen that these borides exhibit high elastic constants and high hardness as well as low Poisson's ratio, providing evidence that the manganese borides have potentially interesting mechanical properties. By varying boron content from Mn_2B to MnB_4 , the elastic constants and hardness change significantly. In particular, the compound

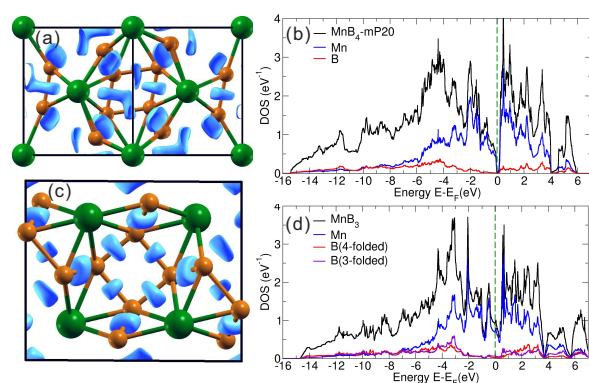


Fig. 6 (color online) (a) and (b) illustrate the isosurface of the electron localization function (ELF) with an isovalue of 0.75 and the calculated density of states of MnB_4 - $mP20$. (c) and (d) illustrate the isosurface of the electron localization function (ELF) with an value of 0.75 and the calculated density of states of MnB_3 .

MnB_4 exhibits the largest shear modulus ($G = 243$ GPa), the highest Pugh's modulus ratio ($k = G/B = 0.885$) and the lowest Poisson ratio of 0.16 which indicates a typical covalently bonding material^{61,62}. The estimated bulk modulus of MnB_4 , 277.9 GPa, is in good agreement with the experimental results, 254(9) GPa⁵⁰. The Vickers hardness of MnB_4 is estimated to be as high as 40.1 GPa. Based on the most recently published experimental measurements⁵⁰, the Vickers hardness of MnB_4 has been found to be 37.4 GPa at a load of 9.8 N and 34.6 GPa at 14.7 N, near the threshold of superhardness, which makes MnB_4 a promising high mechanical performance material. In comparison with MnB_4 , the elastic constant of C_{22} of MnB_3 is just half of its corresponding value, mainly because the 4+8 membered rings of boron in MnB_3 is broken by the removal of some boron atoms from MnB_4 , as discussed above. As expected, the estimated Vickers hardness (32.3 GPa) of MnB_3 is thus lower by about 20% than that of MnB_4 , although MnB_3 is still extremely hard. In addition, it needs to be emphasized that there have been several other theoretical models to derive Vickers hardness^{63–65}. Here, we have attempted to use Gao's model which most fit to covalent and ionic compounds⁶⁵ to calculate Vickers hardness for boron-enriched manganese borides. As illustrated in Table 2, the results are in nice agreement with our currently data. However, because in Mn-rich compounds the metallic feature is highly strong, it is difficult for Gao's model to derive their hardness.

It is well-known that the three-dimensional network of strong covalent bonds is a basic feature of all known hard materials. The high hardness of MnB_3 ($mC16$) and MnB_4 ($mP20$) is consistent with this. As shown in Fig. 6a, the electron localized function (ELF) highlights strong 3D covalent framework of boron and each boron atom is covalently bonded with its four nearest neighboring boron atoms in the quasi-

sp^3 -hybridized configurations with the typical covalent charge accumulations along their boron-boron bonds for MnB_4 . Nevertheless, besides some fourfold boron atoms in the quasi- sp^3 -hybridized configuration in the case of MnB_3 there still exist some three-fold boron atoms in the quasi- sp^2 -hybridized configuration (c.f., Fig. 6c). We have also performed the Bader analysis⁶⁷ of MnB_4 and MnB_3 . It is interesting to note that for MnB_3 each Mn atom loses the charge of about $0.31e$ in average, whereas for MnB_4 the value is about $0.15e$. This fact means that for both MnB_3 and MnB_4 the charges are transferred into boron atoms from Mn atoms. Importantly, the total quantity of the transferred charges from Mn to Boron for MnB_3 is more than that of MnB_4 ($3 \times 0.31e = 0.93e$ for MnB_3 and $4 \times 0.15e = 0.60e$ for MnB_4) to help boron form strong boron-boron covalent bonds and stabilize the boron framework. This results imply that the electronic states of Mn in MnB_4 show a bit more delocalized, as illustrated in the ELF in Fig. 6. Furthermore, the derived electronic densities of states (DOSs) have been compiled in Fig. 6(b and d). For both MnB_3 and MnB_4 , the DOS profiles show nearly pure-boron regions which correspond to the strong boron-boron covalent bonds. In the energy range from -6 eV to -2 eV, the relatively strong electronic hybridizations between boron p -like and Mn d -like have been observed. The nonbonding states basically appear in the energy range from -2 eV to the Fermi level. Interestingly, it can be seen that for MnB_4 the Fermi level sits exactly the deep pseudogap with a nearly zero density, evidencing its electronic stability. However, in the case of MnB_3 the Fermi level locates at the local peak with the DOS value as high as 0.95 states eV^{-1} atom $^{-1}$, resulting in a relatively large electronic specific heat coefficient of $\gamma \approx 3.4$ mJ $^{-1}$ mol $^{-1}$ K $^{-2}$.

5 Conclusions

In summary, through first-principles calculations and variable-composition evolutionary calculations as well as the proper experimental synthesis and the first-principles calculations, we have uncovered four viable ground state compounds, with Mn_2B , MnB , MnB_4 and previously never reported MnB_3 compositions, and two metastable compounds of MnB_2 and Mn_3B_4 . Besides all experimental observations of those borides, our calculations demonstrated that the early characterized $mC10$ structure of MnB_4 should be superceded by the $mP20$ structure predicted and confirmed by our experiment. The previously never observed MnB_3 has been confirmed experimentally to crystallize in the monoclinic $mC16$ structure, in agreement with predictions.

Methodologically, our study highlights the need to re-check the even well-defined known metallic borides, nitrides, and carbides, given the fact both MnB_4 and our recently published CrB_4 ¹² and WB_{3+x} ⁸ were characterized, inaccurately, in the earlier literature. This type of problem was mainly caused by

the weak scattering of X-rays for light elements (*i.e.* B, N, C), which become masked by heavier atoms in the compounds, and consequently, powder XRD is almost blind to the light elements. Therefore, accurate characterization becomes difficult for those compounds if only based on the powder XRD pattern which has been the most extensively used method. To this end, the universal variable-composition predictor, USPEX, which performed extremely successfully as shown for this Mn-B system, provides a powerful method to resolve those problems, opening a new horizon for material discovery and characterization.

Acknowledgement We are grateful for supports from the “Hundred Talents Project” of Chinese Academy of Sciences and from NSFC of China (Grand Number: 51074151) as well as Beijing Supercomputing Center of CAS (including its Shenyang branch. Financial support from DARPA (Grants No. W31P4Q1310005 and No. W31P4Q1210008), National Science Foundation (EAR-1114313, DMR-1231586), CRDF Global (UKE2-7034-KV-11), Government of the Russian Federation (No. 14.A12.31.0003 and No. W31P4Q1310005) and Russia Ministry of Education and Science (No.8512) is gratefully acknowledged.

References

- 1 A. R. Oganov (Editor), in *Modern Methods of Crystal Structure Prediction*, Wiley, 2011.
- 2 S. Curtarolo, W. Setyawan, G. L. W. Hart, M. Jahnatek, R. V. Chepulskii, R. H. Taylor, S. Wang, J. Xue, K. Yang, O. Levy, M. J. Mehl, H. T. Stokes, D. O. Demchenko and D. Morgan, *Comput. Mat. Sci.*, 2012, **58**, 218-226.
- 3 A. R. Oganov, J. Chen, C. Gatti, Y. Ma, Y. Ma, C. W. Glass, Z. Liu, T. Yu, O. O. Kurakevych and V. L. Solozhenko, *Nature*, 2009, **457**, 863-867.
- 4 G. Ceder, *Mater. Res. Soc. Bull.*, 2010, **35**, 693-701.
- 5 S. Wang, Z. Wang, W. Setyawan, N. Mingo and S. Curtarolo, *Phys. Rev. X*, 2011, **1**, 021012.
- 6 K. S. Yang, W. Setyawan, S. D. Wang, M. B. Nardelli and S. Curtarolo, *Nature Materials*, 2012, **11**, 614-619.
- 7 H. Y. Niu, X.-Q. Chen, S. B. Wang, D. Z. Li and Y. Y. Li, *Phys. Rev. Lett.*, 2012, **108**, 135501.
- 8 X. Y. Cheng, W. Zhang, X.-Q. Chen, H. Y. Niu, P. T. Liu, K. Du, G. Liu, D. Z. Li, H.-M. Cheng, H. Q. Ye and Y. Y. Li, *Appl. Phys. Lett.*, 2013, **103**, 171903.
- 9 Q. Gu, G. Krauss and W. Steurer, *Adv. Mater.*, 2008, **20**, 3620-3626.
- 10 R. Mohammadi, A. T. Lech, M. Xie, B. E. Weaver, M. T. Yeung, S. H. Tolbert and R. B. Kaner, *P Natl Acad Sci Usa*, 2011, **108**, 10958-10962.
- 11 R. Mohammadi, M. Xie, A. T. Lech, C. L. Turner, A.

- Kavner, S. H. Tolbert and R. B. Kaner, *J. Am. Chem. Soc.*, 2013, **134**, 20660-20668.
- 12 H. Y. Niu, J. Q. Wang, X.-Q. Chen, D. Z. Li, Y. Y. Li, P. Lazar, R. Podloucky and A. N. Kolmogorov, *Phys. Rev. B*, 2012, **85**, 144116.
- 13 H.-Y. Chung, M. B. Weinberger, J. B. Levine, A. Kavner, J.-M. Yang and S. H. Tolbert, *Science*, 2007, **316**, 436-439.
- 14 J. B. Levine, S. L. Nguyen, H. I. Rasool, J. A. Wright, S. E. Brown, R. B. Kaner, *J. Am. Chem. Soc.*, 2008, **130**, 16953.
- 15 X.-Q. Chen, C. L. Fu, M. Krčmar, G. S. Painter, *Phys. Rev. Lett.*, 2008, **100**, 196403.
- 16 A. N. Kolmogorov, S. Shah, E. R. Margine, A. F. Bialon, T. Hammerschmidt and R. Drautz, *Phys. Rev. Lett.*, 2010, **105**, 217003.
- 17 J. B. Levine, S. H. Tolbert and R. B. Kaner, *Adv. Funct. Mater.*, 2009, **19**, 3519-3533.
- 18 A. L. Ivanovskii, *Prog. Mater. Sci.*, 2012, **57**, 184-228.
- 19 A. F. Bialon, T. Hammerschmidt, R. Drautz, S. Shah, E. R. Margine and A. N. Kolmogorov, *Appl. Phys. Lett.*, 2011, **98**, 081901.
- 20 H. Y. Guo, N. Dubrovinskaia, E. Bykova, A. A. Tsirlin, D. Kasinathan, A. Richter, M. Merlini, M. Hanfland, A. M. Abakumov, D. Batuk, G. V. Tendeloo, Y. Nakajima, A. V. Kolmogorov, L. Dubrovinsky, *Phys. Rev. Lett.*, 2013, **111**, 157002.
- 21 A. N. Kolmogorov, S. Shah, E. R. Margine, A. K. Kleppe and A. P. Jephcoat, *Phys. Rev. Lett.*, 2012, **109**, 075501.
- 22 O. Kkamamoto, *J. Phase Equil.*, 1993, **14**, 121-122.
- 23 B. Aronsson and A. Aselius, *J. Acta Chem. Scand.*, 1958, **12**, 1476-1480.
- 24 L.-E. Terenius, *J. Less-Common Met.*, 1981, **82**, 335-340.
- 25 R. Kiessling, *Acta Chem. Scand.*, 1950, **4**, 146-159.
- 26 B. Aronsson, *Acta Chem. Scand.*, 1960, **14**, 1414-1418.
- 27 S. Andersson, J.-O. Carlsson, *Acta Chem. Scand.*, 1970, **24**, 1791-1799.
- 28 P. K. Liao and K. E. Spear, *Bull. Alloy Phase Diag.*, 1986, **1**, 543-549.
- 29 J. Fan, K. Bao, X. L. Jin, X. X. Meng, D. F. Duan, B. B. Liu and T. Cui, *J. Mater. Chem.*, 2012, **22**, 17630-17635.
- 30 A. Aydin and M. Simsek, *Phys. Rev. B*, 2009, **80**, 134107.
- 31 X. X. Meng, K. Bao, P. W. Zhu, Z. He, Q. Tao, J. J. Li, Z. P. Mao and T. Cui, *J. Appl. Phys.*, 2012, **111**, 112616.
- 32 B. Wang, X. Li, Y. X. Wang, Y. F. Tu, *J. Phys. Chem.*, 2011, **115**, 21429-21435.
- 33 H. Y. Gou, Z. P. Li, H. Niu, F. M. Gao, J. W. Zhang and R. C. Ewing, *Appl. Phys. Lett.*, 2012, **100**, 111907.
- 34 H. Y. Gou, G. Steinle-Neumann, E. Bykova, Y. Nakajima, N. Miyajima, Y. Li, S. V. Ovsyannikov, L. S. Dubrovinsky and N. Dubrovinskaia, *Appl. Phys. Lett.*, 2013, **102**, 061906.
- 35 A. R. Oganov and C. W. Glass, *J. Chem. Phys.*, 2006, **124**, 244704.
- 36 A. R. Oganov, A. O. Lyakhov and M. Valle, *Acc. Chem. Res.*, 2011, **44**, 227-237.
- 37 A. O. Lyakhov, A. R. Oganov, H. T. Stokes and Q. Zhu, *Comput. Phys. Commun.*, 2013, **184**, 1172-1182.
- 38 A. R. Oganov, Y. Ma, A. O. Lyakhov, M. Valle and C. Gatti, *Rev. Mineral. Geochem.*, 2010, **71**, 271-298.
- 39 G. Kresse and J. Furthmüller, *Phys. Rev. B*, 1996, **54**, 11169-11186.
- 40 G. Kresse and J. Furthmüller, *Comput. Mat. Sci.*, 1996, **6**, 15-50.
- 41 J. P. Perdew, K. Burke and M. Ernzerhof, *Phys. Rev. Lett.*, 1996, **77**, 3865-3868.
- 42 S. H. Vosko, L. Wilk and M. Nusair, *Can. J. Phys.*, 1980, **58**, 1200-1211.
- 43 H. J. Monkhorst and J. D. Pack, *Phys. Rev. B*, 1976, **13**, 5188-5192.
- 44 G. Will and B. Z. Kiefer, *Anorg. Allg. Chem.*, 2001, **627**, 2100-2104.
- 45 A. C. Lawson, Allen C. Larson, M. C. Aronson, S. Johnson, Z. Fish, P. C. Canfield, J. D. Thompson and R. B. Von Dreele, *J. Appl. Phys.*, 1994, **76**, 7049-7051.
- 46 A. Togo, F. Oba and I. Tanaka, *Phys. Rev. B*, 2008, **78**, 134106.
- 47 T. Kanaizuka, *J. Solid State Chem.*, 1982, **41**, 195-204.
- 48 G. Papesch, H. Nowotny and F. Bensovsky, *Monatsh. Chem.*, 1973, **104**, 933-942.
- 49 P. Mohn, D. G. Pettifor, *J. Phys. C. Solid State Phys.*, 1988, **21**, 2829-2839.
- 50 H. Y. Gou, A. A. Tsirlin, E. Bykova, A. M. Abakumov, G. Van Tendeloo, A. Richter, S. V. Ovsyannikov, A. V. Kurnosov, D. M. Trots, Z. Konôpková, H.-P. Liermann, L. Dubrovinsky and N. Dubrovinskaia, *Phys. Rev. B*, 2014, **89**, 064108.
- 51 A. Knappschneider, C. Litterscheild, N. C. George, J. Brögoch, N. Wagner, J. Beck, J. A. Kurzman, R. Seshadri and B. Albert, *Angew. Chem. Int. Ed.*, 2014, **53**, 1684-1688.
- 52 M. Yang, Y. C. Wang, J. L. Yao, Z. P. Li, J. Zhang, L. L. Wu, H. Li, J. W. Zhang and H. Y. Gou, *J. Solid State Chem.*, 2014, **213**, 52-56.
- 53 E. Legrand and S. Neov, *Solid State Commun.*, 1972, **10**, 883-885.
- 54 K. Umeno, R. M. Wentzcovitch, S. Saito, T. Miyake, *Phys. Rev. Lett.*, 2010, **104**, 125504.
- 55 A. G. Van Der Geest and A. G. Kolmogorov, 2013, arxiv:1210.4157.
- 56 W. Voigt, *Lehrbuch der Kristallphysik*, Teubner: Leipzig, 1928, 313-315.

-
- 57 A. Z. Reuss, *Angew. Math. Mech.*, 1929, **9**, 49-58.
- 58 R. Hill, *Proc. Phys. Soc.(London)*, 1952, **65**, 349-354.
- 59 X.-Q. Chen, H. Y. Niu, D. Z. Li and Y. Y. Li, *Intermetallics*, 2011, **19**, 1275-1281.
- 60 X.-Q. Chen, H. Y. Niu, C. Franchini, D. Z. Li and Y. Y. Li, *Phys. Rev. B*, 2011, **84**, 121405.
- 61 H. Y. Niu, X.-Q. Chen, P. T. Liu, W. W. Xing, X. Y. Cheng, D. Z. Li and Y. Y. Li, *Scientific Reports*, 2012, **2**, 718.
- 62 S. F. Pugh, *Philos. Mag.*, 1954, **45**, 823-843.
- 63 A. Simunek, and Jiri Vackar, *Phys. Rev. Lett.*, 2006, **96**, 085501.
- 64 K. Y. Li, X. T. Wang, F. F. Zhang, and D. F. Xue, *Phys. Rev. Lett.*, 2008, **100**, 235504.
- 65 F. M. Gao, J. L. He, E. D. Wu, S. M. Liu, D. L. Yu, D. C. Li, S. Y. Zhang, and Y. J. Tian, *Phys. Rev. Lett.*, 2003, **91**, 015502.
- 66 W. J. Zhao, and B. Xu, *Computational Materials Science*, 2012, **65**, 372-376.
- 67 R. F. W. Bader, in *Atoms in Molecules. A Quantum Theory*, Oxford Univ. Press, Oxford, 1990.

Table 1 DFT formation enthalpies (ΔH in eV/atom), optimized lattice parameters and Wyckoff sites the manganese borides searched by USPEX

Phase	Person symbol	Prototype	ΔH	Space group cell	Atom	Wyckoff position	x	y	z
α -Mn ₂ B	oF48	Mg ₂ Cu	-0.4055	<i>Fddd</i>	Mn	16f	0.125	0.4531	0.125
				a=4.1406	Mn	16g	0.125	0.125	0.0438
				b=7.1489 c=14.2770	B	16g	0.125	0.125	0.5011
β -Mn ₂ B	tI12	Al ₂ Cu	-0.3993	<i>I4/mcm</i>	Mn	8h	0.1591	0.6591	0.5
				a=5.0665	B	4a	0.0	0.0	0.25
				b=5.0665 c=4.1104					
α -MnB	oC8	CrB	-0.4924	<i>Cmcm</i>	Mn	4c	0.0	0.3571	0.25
				a=2.9720	B	4c	0.0	0.0683	0.25
				b=7.6151 c=2.9599					
β -MnB	oP8	FeB	-0.4996	<i>Pnma</i>	Mn	4c	0.1746	0.25	0.6232
				a=5.4587	B	4c	0.0334	0.25	0.1149
				b=2.9838 c=4.1263					
Mn ₃ B ₄	oI14	Ta ₃ B ₄	-0.4035	<i>Immm</i>	Mn	2a	0.0	0.0	0.0
				a=2.9314	Mn	4j	0.5	0.0	0.1826
				b=3.0020	B	4j	0.0	0.0	0.4321
				c=12.6771	B	4j	0.5	0.0	0.3542
Mn ₃ B ₄	tP7	Mn ₃ B ₄	-0.4162	<i>P4m2</i>	Mn	1d	0.0	0.0	0.5
				a=2.9684	Mn	2g	0.0	0.5	0.1283
				b=2.9684	B	2f	0.5	0.5	0.3651
				c=6.3734	B	2g	0.0	0.5	0.7849
MnB ₂	hP3	AlB ₂	-0.2831	<i>P6/mmm</i>	Mn	1a	0.0	0.0	0.0
				a=2.9868	B	2d	0.3333	0.6667	0.5
				b=2.9868 c=2.9418 $\gamma=120^\circ$					
MnB ₂	hP6	ReB ₂	-0.3648	<i>P6₃/mmm</i>	Mn	2c	0.3333	0.6667	0.25
				a=2.7784	B	4f	0.3333	0.6667	0.5517
				b=2.7784 c=6.9539 $\gamma=120^\circ$					
MnB ₃	mC16	MnB ₃	-0.3268	<i>C2/m</i>	Mn	4i	0.2899	0.0	0.7958
				a=7.1372	B	4i	0.0070	0.0	0.7127
				b=2.8367	B	4i	0.1771	0.0	0.4735
				c=5.9092 $\beta=90.3629^\circ$	B	4i	0.4275	0.0	0.1194
MnB ₄	mC10		-0.2711	<i>C2/m</i>	Mn	2a	0.0	0.0	0.0
				a=5.4946	B	8j	0.2027	0.3408	0.2026
				b=5.3754 c=2.9532 $\beta=122.51^\circ$					
MnB ₄	mP20		-0.2890	<i>P2₁/c</i>	Mn	4e	0.2230	0.4995	0.2706
				a=5.4717	B	4e	0.1251	0.1805	0.1293
				b=5.3567	B	4e	0.3422	0.3695	0.8372
				c=5.4384	B	4e	0.1384	0.3138	0.6357
				$\beta=114.75^\circ$	B	4e	0.3244	0.1304	0.3291

Table 2 Calculated elastic constants (in GPa), bulk modulus B (in GPa), shear modulus G (in GPa), Young's modulus E (in GPa), Poisson's ratio (ν), Puch's modulus ratio (G/B) as well as the estimated Vickers hardness (H_v , in GPa) of the Mn-B system. The calculated bulk (B), shear (G) and Young's moduli (E) are estimated by the Voight-Reuss-Hill averages⁵⁶⁻⁵⁸. The Vickers hardness estimates (H_v) are obtained with our proposed formula using the calculated elastic moduli^{59,60}.

	α -Mn ₂ B	β -Mn ₂ B	α -MnB	β -MnB	Mn ₃ B ₄	Mn ₃ B ₄	MnB ₂	MnB ₂	MnB ₃	MnB ₄	MnB ₄
	oF40	tI12	oC8	oP8	oI14	oP7	hP3	hP6	mC16	mS10	mP20
C_{11}	592.7	534.6, 535 ^b	389.7	414.4	300.8	341.0	615.4	495.2, 488 ^b	333.9	549.3, 540 ^a	561.7
C_{22}	564.5		521.9	527.7	432.5				455.1	957.6, 954 ^a	871.4
C_{33}	585.8	519.6, 494 ^b	498.1	504.8	526.8	426.9	393.6	867.3, 864 ^b	468.3	531.4, 531 ^a	542.2
C_{44}	138.9	223.9, 219 ^b	182.9	215.8	161.7	148.3	122.1	276.4, 276 ^b	164.8	238.9, 239 ^a	232.0
C_{55}	206.1		215.0	218.4	188.5				305.5	243.6, 245 ^a	211.7
C_{66}	158.7	168.0, 168 ^b	222.0	175.8	116.4	153.4	223.5	164.1, 158 ^b	251.7	170.8, 177 ^a	239.6
C_{12}	173.7	230.9, 222 ^b	137.5	171.1	263.1	227.0	168.4	167.0, 170 ^b	42.0	58.3, 60 ^a	93.2
C_{13}	196.9	211.0, 216 ^b	167.5	147.5	226.4	234.1	111.7	96.4, 99 ^b	176.2	121.8, 126 ^a	107.7
C_{23}	196.9		149.3	127.7	166.6				175.4	90.0, 102 ^a	84.5
C_{15}									10.5	3.67	4.3
C_{25}									-22.4	14.1	-0.03
C_{35}									49.5	13.9	-13.3
C_{46}									17.8	-7.7	6.4
G	177.0	183.0, 201 ^b	182.8	186.0	115.7	108.7	168.6	232.7, 237 ^b	185.9	240.9, 274 ^a	245.0
B	319.7	321.5, 319 ^b	266.2	259.1	280.1	275.7	259.9	281.4, 289 ^b	218.0	279.8, 282 ^a	277.9
E	448.3	461.4, 498 ^b	446.2	450.2	305.2	288.2	415.8	547.2, 559 ^b	434.3	561.5, 621 ^a	568.1
ν	0.27	0.26, 0.24 ^b	0.22	0.21	0.32	0.33	0.23	0.18, 0.18 ^b	0.17	0.17, 0.13 ^a	0.16
G/B	0.55	0.57, 0.63 ^b	0.69	0.72	0.41	0.39	0.65	0.83, 0.82 ^b	0.85	0.86, 0.97 ^a	0.88
H_v	17.7	18.8	24.1	25.8	8.5	7.5	21.2	35.8	32.3	38.5	40.1
H_{Gao}							16.5 ^b	40.3 ^b	39.5	49.9 ^b	48.7

^a Reference 66, ^b Reference 32

Variable-composition evolutionary algorithm calculations combined with first-principles calculations have uncovered four viable ground compounds, Mn_2B , MnB , MnB_4 and previously never reported MnB_3 , in the well-known Mn-B binary. Surprisingly, the early characterized and long-believed $m\text{C}10$ structure of MnB_4 is dynamical unstable and instead, the real crystal structure ($m\text{P}20$) of MnB_4 is clarified and further confirmed by experiment.

